Polarization-Independent Linear Waveguides in 3D Photonic Crystals

E. Lidorikis, M. L. Povinelli, S. G. Johnson, and J. D. Joannopoulos

Department of Physics, Massachusetts Institute of Technology, Cambridge, Massachusetts 02139, USA

Using a symmetry-based approach, we have designed polarization-independent waveguides in a 3D photonic crystal. A comprehensive series of numerical experiments, involving the propagation of pulsed signals through long straight waveguide sections and sharp bends, quantitatively evaluates the bend-transmission coefficient over the entire bandwidth of the corresponding guided modes. High ($\sim 95\%$) polarization-independent bend transmission is achieved within a certain frequency range.

Lossless guiding of light at length scales approaching the wavelength of the light itself is a necessary property for any future integrated optical circuit. While high index-contrast dielectric waveguides can reduce radiation losses from features such as sharp bends [1,2], they cannot completely suppress them and are in general very sensitive to roughness. Photonic crystals [3,4], on the other hand, have been shown in certain cases to eliminate radiation loss [5,6] and thus offer a promising platform for designing high-performance waveguide networks. A common drawback, however, to all photonic-crystal waveguide systems proposed until now (2D [7–10] or 3D [11,12] systems), is that they are highly polarization selective. Given that the polarization state of an input signal may not be known and/or may vary over time, their proper operation would require the use of active polarization preprocessing devices. In this work, we demonstrate that, by utilizing the symmetries of a proper choice of 3D photonic crystal [13], one can tune line defects to create guided modes inside the spectral gap that are essentially degenerate, with a polarization-insensitive dispersion relation. We further demonstrate the stability of these modes to symmetry breaking by simulating high-transmission polarization-independent light guiding around a sharp bend. To our knowledge, this is the first time such polarization-insensitive transmission has been obtained at such length scales.

One approach to polarization insensitivity would be to design a photonic crystal with line defects possessing the appropriate cross-sectional symmetry for polarization degeneracy. Another approach is to employ a photonic crystal consisting of two kinds of photonic-crystal slabs, each best suited for confining one of two possible polarizations. The latter approach results in planar arrays of defects, which are amenable to microfabrication, and is the method used here. The photonic crystal of Ref. [13] provides precisely this capability, consisting of alternating slabs of dielectric rods in air (*rod* layers, appropriate for confining TM-polarized waves) and air holes in dielectric (*hole* layers, appropriate for confining TE-polarized waves). Waveguiding structures can be designed within this crystal by introducing planar line defects in the *hole* and/or *rod* layers, resulting in the formation of defect (guided) bands inside the band gap [14]. A remarkable property of this 3D crystal is that the resulting guided modes are very similar to the 2D TE- and TM-polarized modes one gets from solving a 2D problem with the dielectric constant defined by the corresponding cross section along the defect plane [14]. Hence, in the 3D crystal, a sequence of larger holes in a *hole* layer results in a TE-like mode pulled up from the dielectric band, predominantly polarized with its magnetic field normal to the defect plane. Similarly, a sequence of smaller rods in a *rod* layer also results in a TM-like mode pulled up from the dielectric band, but now predominantly polarized with its electric field normal to the defect plane. Note that these modes are approximately even (TE) and odd (TM) under reflection on a plane parallel to the *hole* and *rod* layers. In a purely 2D system, this symmetry is exact, prohibiting mode mixing even at lattice distortions such as bends or disorder. This is a key criterion needed to induce a significant suppression of mode mixing at similar planar lattice distortions.

Because of the omnidirectional gap provided by the photonic crystal, the above procedure enables the design of wavelength-scale minimal-loss waveguide networks for both polarizations. While this is promising for integrated optical systems, still, it does not overcome one of integrated optics' old problems: Each polarization satisfies a different dispersion relation, resulting in different propagation properties such as speed and pulse broadening, thus leading to a different response in any device. However, if we combine the two sequences of line defects in a way so that the two guided modes are close spatially yet maintain different symmetry, we may tailor the defect structures to enforce an ''accidental degeneracy'' in the guided dispersion relations, i.e., to have them coincide. In this regard, it is important to identify a symmetry operation along the guide direction, with respect to which the two modes (eigenstates) transform oppositely, so that a tailored defect structure respecting this symmetry will not result in mode mixing and repulsion.

A portion of our structure consisting of two layers is shown in Fig. 1. We create our waveguides along the set of
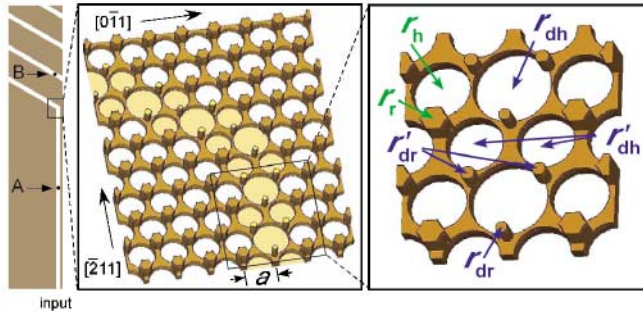
FIG. 1 (color). A schematic of the simulation system and two successive blowups, one involving the greater bend area and the other just a small straight part of the waveguide (green/blue denotes bulk/defect radii). Only the two layers of the 3D crystal involving the planar line defects are shown for clarity (defect holes and rods are highlighted in yellow in the middle frame). The waveguide, defined by the white line, "wraps around" after the bend using periodic boundary conditions, minimizing the required computational cell. Monitor points are at A and B.

$\{[\bar{2}11]\}$ (second nearest neighbor) directions, because there is a mirror plane perpendicular to the layers, lying along the axis of a straight $\{[\bar{2}11]\}$ waveguide, for both the *hole-* and *rod-layer* line defects. This distinguishes the TE-like and TM-like modes into different irreducible representations. In contrast, had we chosen a waveguide along the $\{[0\bar{1}1]\}$ (nearest neighbor) directions, the only symmetry operation that leaves both the *hole-* and *rod-layer* line defects invariant is a 180° rotation along $\{[0\bar{1}1]\}$. However, this operation cannot distinguish between TE-like and TM-like modes.

The detailed structure of the photonic-crystal is reported in Refs. [13,14]. The hole radius within the *hole* layer is $r_h = 0.414a$ and the equivalent-rod [14] radius within the *rod* layer is $r_r = 0.175a$, where a is the in-plane lattice constant and is related to the fcc lattice constant a_{fcc} by $a = a_{\text{fcc}}/\sqrt{2}$. We use a dielectric contrast of 12, for which a band gap of 21% is obtained. The first step is to introduce two line defects to create two guided modes of opposite polarization: larger holes ($r_{dh} = 0.53a$) in the *hole* layer (which will support the TE-like odd mode) and smaller rods ($r_{dr} = 0.08a$) in the *rod* layer (which will support the TM-like even mode). The dispersion relations of these two modes, calculated by the finite-difference time-domain (FDTD) method [15], are shown in Fig. 2(a). They differ in both their center frequency and their bandwidth. A key property, however, is that they are both well described by a cosine dispersion relation, which makes them easier to match. This cosine dispersion relation arises because our waveguides are very similar to a chain of weakly coupled defects. For stronger coupling, it is expected that the dispersion relations will divert from the simple cosine form and it will thus become progressively difficult to match them. We will use these two bands as a starting point and perturb the surrounding crystal elements (i.e., other holes and rods in the vicinity) to force accidental degeneracy.
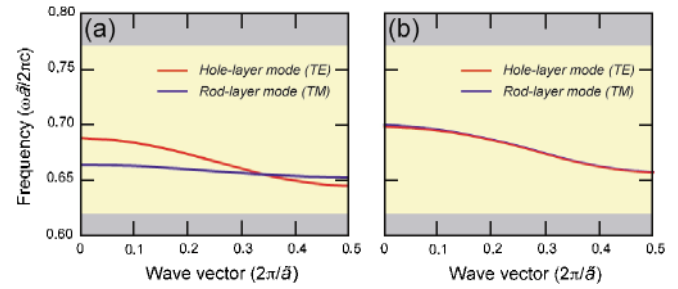
FIG. 2 (color). Dispersion relations for the guided modes resulting from planar line defects in the 3D photonic crystal, (a) before and (b) after the tuning. Gray areas mark transmission bands while yellow areas mark band gaps.

For simplicity, we limit ourselves to changes in radius only. Such changes effectively add or remove dielectric material from the high field-intensity regions, thus introducing a shift in the corresponding dispersion relation. We adopt an empirical approach where we fit the effect of different radius perturbations, and combine them through a conjugate-gradient search algorithm to find the combination producing the desired degeneracy. By combining two perturbations per layer, we find a range of defect parameters that result in degenerate bands, each at a different center frequency and bandwidth. A parameter set requiring small radius changes is $r_{dh} = 0.55a$, $r'_{dh} = 0.40a$, $r_{dr} = 0.085a$, and $r'_{dr} = 0.10a$ for the two hole and rod radii, respectively (see Fig. 1). The corresponding dispersion relations demonstrating the degeneracy are shown in Fig. 2(b) (additional bands are slightly pulled up from the "dielectric" band as well, but are not shown here since they do not come close to our modes of interest). The resulting "doubly degenerate" guided mode has a bandwidth of about 6% of its center frequency and a group velocity at the Brillouin-zone center of about $0.13c$. To our knowledge, this is the first time a polarization-independent dispersion relation has been demonstrated for a linear waveguide in a 3D photonic-crystal structure.

A natural and important question is to what degree this degeneracy maintains a polarization-independent response in cases where we break symmetry, such as at a sharp bend. To answer this, we study a system that involves a 60° bend, as depicted in Fig. 1. Note that the two layers are not equivalent at the bend. While in the *hole-layer* structure we have a smooth transition between the two straight waveguide branches, in the *rod-layer* the bend creates a nearest neighbor coupling of two rods of radius r_{dr} (normally second-nearest-neighbor coupling in the straight waveguide). In fact, there is no way to make both layers have a smooth transition between their two branches. As we shall see, this introduces slightly different high-transmission resonance conditions for each polarization. In addition, there will be some mixing between the two polarization states at the bend, where the mirror symmetry is destroyed.

We use the FDTD method to simulate the propagation of electromagnetic pulses through the bend. The computational system is taken very large to assure clear separation among the various pulses. It consists of a cell of size $72\tilde{a} \times 16a \times 2a_v$, where $\tilde{a}$ is the lattice period along the propagation direction, $\tilde{a} = \sqrt{3}a = \sqrt{3/2}a_{\text{fcc}}$, and a_v is the lattice period along the vertical [111] direction (three bilayers), $a_v = \sqrt{6}a = \sqrt{3}a_{\text{fcc}}$. The bend is located at a distance of $48\tilde{a}$ from the entrance of the input waveguide. We use perfectly matched-layer boundary conditions [16] in the propagation direction, and periodic boundary conditions in the other two directions. The waveguide region after the bend is "wrapped around" using the periodic boundary conditions, minimizing the required size of the computational cell.

A pulse with a Gaussian profile in time is launched at the entrance of the waveguide, and the fields are monitored at two positions, as shown in Fig. 3. Position A is located halfway between the source and the bend and is the observation point for the incident and reflected pulses, while position B is located $12\tilde{a}$ after the bend and is the observation point for the transmitted pulse (see Fig. 2). Minimal secondary reflections at the edges of the computational cell are still present, but they appear at later times and do not contaminate the useful data. We find that most of the energy is transmitted through the bend. As expected, the symmetry breaking at the bend results in transmitted and reflected pulses that are composed of both modes. However, this mixing is very small, comparable to half the overall reflection from the bend (see Fig. 3).

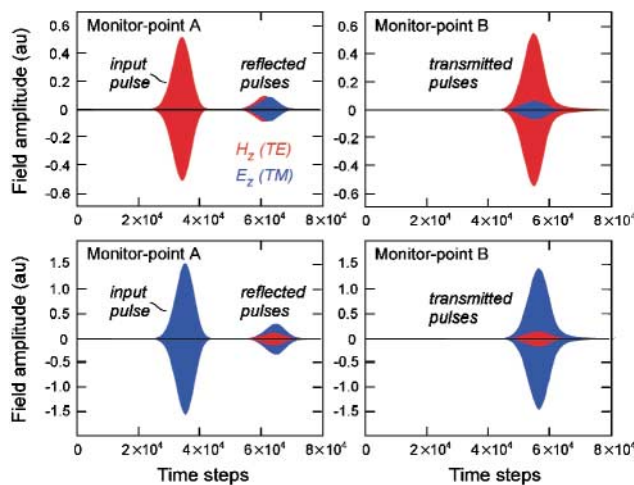In order to quantify the transmission through the bend, we study the frequency-resolved pulses going in and out of the bend. Since these are not single-mode waveguides, we must use data from flux-monitoring planes, positioned at A and B. For better resolution, as well as a consistency test, we use two pulses of different center frequencies per polarization, as shown in the top panels of Fig. 4. The corresponding ratios of the fluxes at A and B provide the transmission and reflection coefficients, as shown in the bottom panel of Fig. 4. These coefficients add up to 1 for all frequencies, with an error of less than 1%. We find a wide frequency range of high transmission for both modes, and a frequency $\omega\tilde{a}/2\pi c = 0.6835$ for which the transmissions coincide to 94.5%. Note that, as expected, resonant transmission is observed at different frequencies for the two modes: at lower frequencies for the TE-like mode and higher frequencies for the TM-like mode. Also note that the TM mode does not actually achieve 100% transmission at any frequency within the useful bandwidth. Further tuning of the bend region could lead to 100% transmission of this mode if desired.

Around the common transmission frequency, we resolve the calculated fluxes into the two modes, in order to quantify the degree of modal mixing. We find that mixing is generally small, and that it monotonously decreases for increasing frequency (from about 5% at $\omega\tilde{a}/2\pi c = 0.675$ to less than 1% at $\omega\tilde{a}/2\pi c = 0.69$). At the common high-transmission frequency, the transmitted power retains its polarization to about 97%. The absence of strong modal mixing is due to the approximate horizontal mirror plane symmetry, as was mentioned earlier. In Fig. 5, we plot the field patterns of the propagating modes, obtained by launching suitable continuous-wave (cw) signals. In the right panels, we show the corresponding vertical cross

FIG. 3 (color). Fields at the observation points A and B, which are located before and after the bend, respectively. Each polarization is studied separately with points A and B centered in the appropriate layer in each case. Red is used for the H_z field of the TE-like mode and blue for the E_z field of the TM-like mode. A pure TE(TM)-like mode will have zero E_z (H_z) field at its symmetric center, as is the case for the incident pulses.
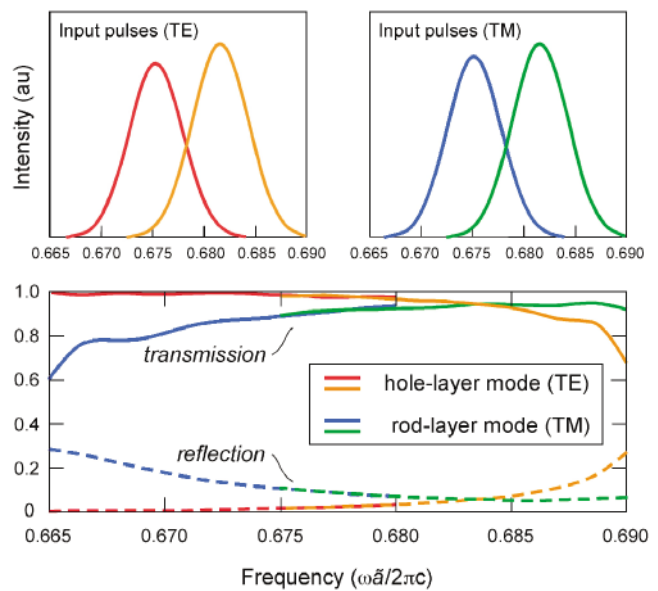

FIG. 4 (color). Top panels: Spectral profile of the input pulses used in the numerical experiments for the TE-like and the TM-like modes. Bottom panel: By taking appropriate ratios of transmitted, reflected, and input pulses, we extract the corresponding transmission and reflection coefficients.
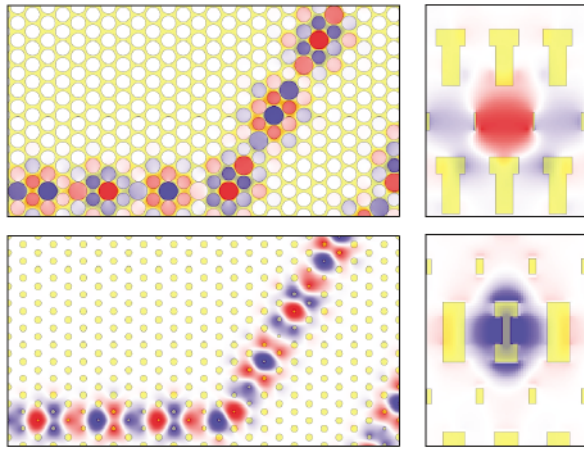
FIG. 5 (color). Lateral and vertical modal profiles for a cw excitation at the common high-transmission frequency for the TE-like mode (top panels) and the TM-like mode (bottom panels), where the H_z and E_z fields are plotted, respectively. Yellow areas correspond to the high dielectric part of the structure.

sections, where the effects of the approximate symmetry become apparent. The TE-like and TM-like modes appear as two different representations of a single horizontal symmetry plane, thus resulting in minimal mode mixing in the bend region. An important point to note here is that the field pattern of the two modes is different. This will manifest into different coupling coefficients with a symmetric input such as from a fiber. It will thus be necessary to tailor the input part of the waveguides in order to match the coupling coefficients, and thus achieve polarization-insensitive excitation. This, however, goes beyond the scope of this paper.

We have demonstrated high ($\sim$95%) transmission through a sharp bend, with a high degree ($\sim$97%) of polarization insensitivity, for certain frequencies. Two improvements can be achieved by optimizing the crystal structure at the bend: (i) an increase of the symmetry at the bend, so that less mode mixing occurs, and (ii) a change of the resonant-transmission conditions for the two modes so that they better coincide. Thus, there are enough degrees of freedom for optimization that, ultimately, it should be possible to achieve 100% polarization-independent transmission through sharp bends in this system.

In addition to guiding light around sharp corners, such fine-tuned waveguide structures are ideal for miniaturized passive polarization-processing components. Because each polarization is primarily guided in a different layer, it is very easy to separate the two modes. We can easily imagine designing devices such as polarization splitters (each mode bends into a different branch of a junction), or polarization rotators (one mode tunneling to the other by resonant mode mixing). These structures may thus prove to be very useful in future integrated all-optical systems. In contrast, had we employed the

alternative approach of designing a photonic crystal with line defects possessing the appropriate cross-sectional symmetry for polarization degeneracy, such operations would be more difficult, as both modes would be primarily guided by the same crystal elements.

In conclusion, we have shown that polarization-independent waveguides and waveguide bends can be designed in a particular class of 3D photonic crystals by means of forced accidental degeneracy. The only r equirement is the existence of two well-localized modes of definite and opposite symmetry. Further improvements and/or creation of novel polarization-processing devices should be possible by optimizing the structure parameters.

———————

[1] J. S. Foresi, D. R. Lim, L. Liao, A. M. Agarwal, and L. C. Kimerling, Proc. SPIE **3007**, 112 (1997).

[2] C. Manolatou, S. G. Johnson, S. Fan, P. R. Villeneuve, H. A. Haus, and J. D. Joannopoulos, J. Lightwave Technol. **17**, 1682 (1999).

[3] J. D. Joannopoulos, R. D. Meade, and J. N. Winn, *Photonic Crystals* (Princeton, New York, 1995).

[4] For recent work, see, e.g., *Photonic Crystals and Light Localization*, edited by C. M. Soukoulis, Proceedings of the NATO ASI on Photonic Band Gap Materials, Limin Hersonissou, Crete, Greece, 2000 (Kluwer Academic, Dordrecht, 2001).

[5] A. Mekis, J. C. Chen, I. Kurland, S. Fan, P. R. Villeneuve, and J. D. Joannopoulos, Phys. Rev. Lett. **77**, 3787 (1996).

[6] J. D. Joannopoulos, P. R. Villeneuve, and S. Fan, Nature (London) **386**, 143 (1997).

[7] M. Tokushima, H. Kosaka, A. Tomita, and H. Yamada, Appl. Phys. Lett. **76**, 952 (2000).

[8] E. Chow, S. Y. Lin, J. R. Wendt, S. G. Johnson, and J. D. Joannopoulos, Opt. Lett. **26**, 286 (2001).

[9] J. Moosburger, M. Kamp, A. Forchel, S. Olivier, H. Benisty, C. Weisbuch, and U. Oesterle, Appl. Phys. Lett. **79**, 3579 (2001).

[10] A. Talneau, L. Le Gouezigou, N. Bouadma, M. Kafesaki, C.M. Soukoulis, and M. Agio, Appl. Phys. Lett. **80**, 547 (2002).

[11] B. Temelkuran and E. Ozbay, Appl. Phys. Lett. **74**, 486 (1999); M. Bayindir, E. Ozbay, B. Temelkuran, M. M. Sigalas, C. M. Soukoulis, R. Biswas, and K. M. Ho, Phys. Rev. B **63**, 081107(R) (2001).

[12] A. Chutinan and S. Noda, Appl. Phys. Lett. **75**, 3739 (1999); S. Noda, K. Tomoda, N. Yamamoto, and A. Chutinan, Science **289**, 604 (2000).

[13] S. G. Johnson and J. D. Joannopoulos, Appl. Phys. Lett. **77**, 3490 (2000).

[14] M. L. Povinelli, S. G. Johnson, S. Fan, and J. D. Joannopoulos, Phys. Rev. B **64**, 075313 (2001).

[15] K. S. Kunz and R. J. Luebbers, *The Finite-Difference Time-Domain Methods* (CRC, Boca Raton, FL, 1993).

[16] J. C. Chen and K. Li, Microwave Opt. Tech. Lett. **10**, 319 (1995).